The Journal of Immunology

How H13 Histocompatibility Peptides Differing by a Single Methyl Group and Lacking Conventional MHC Binding Anchor Motifs Determine Self-Nonself Discrimination

David A. Ostrov, Matthew M. Roden, Wuxian Shi, Edith Palmieri, Gregory J. Christianson, Lisa Mendoza, Gilbert Villaflor, Darcie Tilley, Nilabh Shastri, Howard Grey, Steven C. Almo, Derry Roopenian and Stanley G. Nathenson

J Immunol 2002; 168:283-289; ;
doi: 10.4049/jimmunol.168.1.283
http://www.jimmunol.org/content/168/1/283

The Journal of Immunology is published twice each month by
The American Association of Immunologists, Inc.,
1451 Rockville Pike, Suite 650, Rockville, MD 20852

Print ISSN: 0022-1767 Online ISSN: 1550-6606.

How H13 Histocompatibility Peptides Differing by a Single Methyl Group and Lacking Conventional MHC Binding Anchor Motifs Determine Self-Nonself Discrimination[1]

David A. Ostrov,* Matthew M. Roden,† Wuxian Shi,* Edith Palmieri,† Gregory J. Christianson,§ Lisa Mendoza,¶ Gilbert Villaflor, ¶ Darcie Tilley,‖ Nilabh Shastri,¶ Howard Grey,‖ Steven C. Almo,[2]* Derry Roopenian,[2]§ and Stanley G. Nathenson[2]†‡

The mouse H13 minor histocompatibility (H) Ag, originally detected as a barrier to allograft transplants, is remarkable in that rejection is a consequence of an extremely subtle interchange, P4$^{Val/Ile}$, in a nonamer H2-D^b-bound peptide. Moreover, H13 peptides lack the canonical P5^{Asn} central anchor residue normally considered important for forming a peptide/MHC complex. To understand how these noncanonical peptide pMHC complexes form physiologically active TCR ligands, crystal structures of allelic H13 pD^b complexes and a P5^{Asn} anchored pD^b analog were solved to high resolution. The structures show that the basis of TCRs to distinguish self from nonself H13 peptides is their ability to distinguish a single solvent-exposed methyl group. In addition, the structures demonstrate that there is no need for H13 peptides to derive any stabilization from interactions within the central C pocket to generate fully functional pMHC complexes. These results provide a structural explanation for a classical non-MHC-encoded H Ag, and they call into question the requirement for contact between anchor residues and the major MHC binding pockets in vaccine design. ***The Journal of Immunology,*** **2002, 168: 283–289.**

The H13 minor histocompatibility (H)[3] Ag provides one of the most subtle examples of self/nonself discrimination. Snell et al. (1) originally detected H13 as a barrier to both tumor and skin allograft transplants, and using histogenetic techniques, isolated this H Ag via the production of H13 congenic mouse strains. Reciprocally reactive CD8$^+$ CTLs can be readily generated by immunization of mice from H13 congenic partner strains. This alloreactivity is conferred by the conservative Val/Ile polymorphism in the naturally processed H2-D^b-bound SSV(V/I) GVWYL nonamer peptide present at fewer than 50 copies per target cell (2). Moreover, because reciprocal CTL responses can be generated, the respective self peptides must act as negatively selecting self ligands in the respective hosts. In keeping with this subtle difference, self/nonself discrimination is incomplete in that H13 self-peptides act as partial agonists. Within the narrow window that distinguishes self from nonself, CTLs are readily generated, leading to the graft rejection phenotype. This model offers a unique opportunity to investigate T cell recognition of naturally processed and presented variant peptides that are responsible for substantial biological activity in vivo: T cell selection leading to allograft rejection.

An equally remarkable facet of the H13 system is that the allelic H13 peptides do not conform to the conventional MHC motif paradigm (3–5). MHC allelic variation gives rise to differential peptide binding due to the presence of polymorphic residues, which give distinct chemical and size characteristics to six pockets (A-F; Refs. 6 and 7) within the peptide binding groove. Allele-specific binding motifs were initially revealed by sequencing peptides eluted from MHC molecules (8, 9). For example, peptides eluted from D^b exhibit XXXXAsnXXXMet/Leu, where X is any amino acid. Both crystallographic and biochemical analyses support the importance of the centrally positioned P5 asparagine (P5^{Asn}) side chain in stabilizing the pD^b complex by forming hydrogen bonds (H-bonds) with C pocket residues Gln^{70}, Gln^{97}, and Tyr^{156} in the Ag binding domain (4, 10). Strikingly, P5 of H13 peptides is glycine (2), which cannot make the canonical contacts or occupy the C pocket of the D^b molecule. To understand how H13 peptides interact and stabilize D^b in the absence of the P5 anchor residue and how T cells distinguish self from nonself based on such subtle antigenic peptide differences, we describe high resolution crystal structures of allelic H13 peptide/D^b complexes, as well as compare them with the structure of a pD^b complex formed with a peptide modified to contain the canonical asparagine anchor residue.

Materials and Methods

Preparation of H2-D^b complexes

Using a method adopted from Young et al. (10), *Escherichia coli* inclusion bodies of H2-D^b and β_2-microglobulin were separately denatured in 8.0 M urea and 20 mM Tris, pH 8.0, and were separately mixed with the synthetically prepared peptides representing the H13 peptides: H13^a, (SSV VGVWYL), H13^b, (SSVIGVWYL), and the P5 analog (SSVVNVWYL) in a mass ratio of 3:1:0.5 in 6 M urea and 20 mM Tris, pH 8.0. These

Departments of *Biochemistry, †Microbiology and Immunology, and ‡Cell Biology, Albert Einstein College of Medicine, Bronx, NY 10461; §The Jackson Laboratory, Bar Harbor, ME 04609; ¶Department of Molecular and Cell Biology, University of California, Berkeley, CA; and ‖The La Jolla Institute for Allergy and Immunology, San Diego, CA 92121

Received for publication August 21, 2001. Accepted for publication October 26, 2001.

The costs of publication of this article were defrayed in part by the payment of page charges. This article must therefore be hereby marked *advertisement* in accordance with 18 U.S.C. Section 1734 solely to indicate this fact.

[1] This work was supported by National Institutes of Health Research Grants AI28802, AI07289, CA09173, AI42970, and RR12408 01A1, by Cancer Center support (CCSG) Grant CA34196, and by the Department of Energy, Offices of Health and Environmental Research and Basic Energy Sciences under contract DE-AC02-98CH10886, by the National Science Foundation, 1P41.

[2] Address correspondence and reprint requests to Dr. Derry Roopenian, The Jackson Laboratory, 600 Main Street, Bar Harbor, ME 04609. E-mail address: dcr@aretha.jax.org; or Dr. Steven C. Almo or Dr. Stanley G. Nathenson, Albert Einstein College of Medicine, 1600 Morris Boulevard, Bronx, NY 10461. E-mail addresses: almo@aecom.yu.edu or nathenso@aecom.yu.edu

[3] Abbreviations used in this paper: H, histocompatibility; H-bonds, hydrogen bonds; SVL9, SSVVGVWYL; SIL9, SSVIGVWYL; SVNL9, SSVVNVWYL.

0022-1767/02/$02.00

mixtures were refolded by dialysis against 10 mM Tris, pH 8.0, at 4°C in Spectra/Por CE dialysis tubing (MWCO 500) for 48 h. The dialysate was subsequently centrifuged at 15,000 × *g* and concentrated (30,000 MWCO; Amicon, Beverly, MA). The supernatant was chromatographed in a buffer containing 20 mM Tris and 150 mM NaCl, pH 8.0, on a Superdex75 column (Pharmacia Biotech, Uppsala, Sweden). Fractions containing the highest concentration of pD^b complexes were pooled from multiple runs, dialyzed against water, and concentrated (30,000 MWCO; Centricon, Bedford, MA). The synthetic peptides were produced by the Peptide Synthesis Facility of the Albert Einstein College of Medicine and Research Genetics (Huntsville, AL) using solid-phase F-moc chemistry, purified by HPLC, and confirmed by mass spectrometric analysis.

Crystallization of the H2-D^b complexes

Crystals were grown using the sparse scan technique (11) with the hanging drop vapor diffusion method. Large single crystals of SVL9/D^b were produced in 12% polyethylene glycol 4000 and 0.1 M HEPES, pH 7.0 from drops incubated at 18°C. SIL9/D^b and SVNL9/D^b crystals were produced in identical conditions except the crystallization buffer also contained 0.2 M sodium acetate. Crystals were observed within 1 day.

Data collection

Crystals were transferred stepwise in reservoir solutions modified to contain up to 20% glycerol as cryoprotectant buffers, and flash cooled at 100 K. Data sets were collected at the X9B beamline at the Albert Einstein Center for Synchrotron Biosciences (National Synchrotron Light Source, Brookhaven National Laboratory, Upton, NY) with a MARCCD detector. Data were indexed, scaled, and merged using the programs DENZO and SCALEPACK (12). All crystals belong to the monoclinic space group C2 with similar unit cell dimensions. Data collection and statistics are reported in Table I. The structure of H13[a] peptide SVL9 (SSVVGVWYL) bound to H2-D^b was solved by molecular replacement with the program AmoRe (13) using the crystal structure of H2-D^b complexed to an influenza virus peptide, Np9, (ASNENMETM; Ref.10; Protein Data Bank identification code 1hoc) as a model. The $\alpha1\alpha2$ domains forming the Ag binding cleft, the $\alpha3$ domain, and β_2-microglobulin were separately fitted by rigid body refinement in XPLOR was subsequently subjected to cycles of anisotropic and bulk solvent correction, simulated annealing refinement, individual B-factor refinement using the program CNS (14) and model adjustment and rebuilding using the program O (15). The structures of SIL9 and SVNL9 were solved by Fournier methods using SVL9 and SIL9, respectively, as starting models. Analysis of the final models show that they have characteristics of well-refined structural models with low values for R_{cryst} and R_{free} and good geometry (16). Coordinates have been deposited in the Protein Data Bank (1INQ).

Structural analysis

Solvent accessibility statistics were calculated with the program DSSP (17) and the Protein-Protein Interaction Server (18). [/ϕ] and Ψ angles were calculated with the program VADAR. H-bond and van der Waals contacts were calculated with the programs HBPLUS (19) and CONTACSYM (20), respectively.

Table I. *Crystallographic analysis and MHC binding capacity of H13 peptides*

Data Set	Data Collection Statistics		
	SVL9	SIL9	SVNL9
Space group	C2	C2	C2
A	92.6	92.0	91.5
B	109.4	109.7	109.8
C	57.6	57.7	58.1
β	120.0	120.5	121.0
Resolution (Å)[a]	2.2 (2.27–2.20)	2.0 (2.07–2.00)	1.9 (1.97–1.90)
Reflections			
Total	109,562	163,125	126,650
Unique	25,365	33,573	38,646
I/σ(I)	24.4 (7.5)	47.6 (15.8)	31.9 (5.3)
Completeness:	99.0 (83.4)	97.3 (75.1)	97.3 (75.9)
R_{sym} (%)[b]	5.8 (19.5)	3.8 (12.9)	3.0 (22.9)
	Refinement Statistics		
Resolution (Å)	20.0–2.2	20–2.0	20.0–1.9
R_{cryst} (%)[c]	20.9	20.5	20.2
R_{free} (%)[d]	26.1	24.2	24.4
Reflections over 2σ			
For refinement	24,403	29,335	32,242
For R_{free}	1,803	3,252	3,575
Protein atoms	3,162	3,165	3,168
Water molecules rms deviations from ideal	123	279	284
Bond lengths (Å)	0.010	0.010	0.010
Angles (°)	1.55	1.47	1.50
	Ramachandran Plot		
Most favored (%)	91.8	90.6	91.9
Additionally allowed (%)	7.6	8.8	7.8
Generously allowed (%)	0.6	0.6	0.3
Disallowed (%)	0.0	0.0	0.0
	D^b Binding Capacity[e]		
Peptide			
LCMV gp33–41	KAVYNFATC	1.000	72
SVL9	SSVVGVWYL	0.160	539
SIL9	SSVIGVWYL	0.060	1,400
SVNL9	SSVVNVWYL	1.830	57

[a] Values in parentheses are for the highest resolution shell.
[b] $R_{sym} = \Sigma_i|I_{hi} - <I_{hi}>|/\Sigma_i|I_{hi}|$, where h specifies unique reflection indices, i indicates symmetry equivalent observations of h.
[c] $R_{cryst} = \Sigma||F_o| - |F_c||/\Sigma|F_o|$ for all reflections, where F_o and F_c are the observed and calculated structure factors, respectively.
[d] R_{free} was calculated against 10% of the reflections removed at random from the refinement.
[e] Shown are the sequence, relative binding affinity, and IC_{50} of peptide binding in nanomoles.

Peptide binding assays

The binding of peptides to D^b molecules was assessed by measuring the amount of peptide required to inhibit by 50% the binding of a known radioligand to soluble purified D^b, as previously described (21).

H13 minigene expression constructs

To determine the effect of amino acid substitutions in the H13 peptide on T cell recognition, minigene constructs were prepared as described (2, 22). Briefly, the minigene constructs were produced to encode Met-SS V(X)GVWYL, Met-SSVVG(X)WYL, or Met-SSVGVY(X)L in which (X) is a random amino acid substitution of the core SSVVGVWYL $H13^a$ peptide.

Cell lines, T cell activation, and cytotoxic assays

Ag-specific responses of T cell hybrids were determined by the production of β-galactosidase (*lacZ*) activity (23). The $H13^a$-specific hybrid 30NX/B10Z and the $H13^b$-specific hybrid B/NXZ have been described (2). In brief, 3–10 × 10^4 cells were cocultured overnight in duplicate with 2–5 × 10^4 LMtk cells cotransfected with H13 minigene constructs, D^b, and B7.2 cDNA. The peptide/MHC-induced T cell response was assayed as *lacZ* activity using the substrate chlorophenol red β-D-galactopyrannoside. The conversion of this substrate to chlorophenol red was measured at 595 and 655 nm as a reference wavelength with a 96-well microplate reader (Bio-Rad, Richmond, CA). To generate bulk anti-$H13^a$ CTLs, B10.CE(30NX)-*H13*^{b}/Sn mice (maintained at The Jackson Laboratory, Bar Harbor, ME) were primed twice with 2 × 10^7 spleen cells from $H13^a$ male C57BL/10Sn (B10) mice, and were then restimulated for 5–6 days with spleen cells from 2000 rad-irradiated female B10 mice in DMEM medium supplemented on day 3 of culture with 10–30 U/ml rIL-2 as described (24). To generate bulk anti-$H13^b$ CTLs, female B10 mice were primed similarly with cells from B10.CE(30NX)-*H13*^{b}/Sn male mice and were restimulated in vitro with cells from female CE(30NX)-*H13*^{b}/Sn mice. Specificity of the CTLs for naturally presented $H13^a$ and $H13^b$ minor H Ags, respectively, was confirmed by conventional cell-mediated lympholysis analysis of female B10.CE(30NX)-*H13*^{b}/Sn and B10 lymphoblast target cells (data not shown). The standard ^{51}Cr release cell-mediated lympholysis assay as described previously was used for assessment of cytotoxic activity against synthetic peptide pulsed target cells (2). The target cells were T2 cells transfected to express H2-D^b, kindly provided by P. Cresswell (Yale University, New Haven, CT). Synthetic peptide-pulsed T2-D^b target cells were prepared by adding 5 × 10^4 ^{51}Cr-labeled target cells to V-bottom microtiter wells carrying varying peptide concentrations for 1 h. Effector cells were then added at E:T ratio of 10:1 or 20:1 and were incubated for 4 h. The percentage of specific lysis was calculated from the amount of ^{51}Cr released into the culture supernatant and is the mean of triplicate cultures.

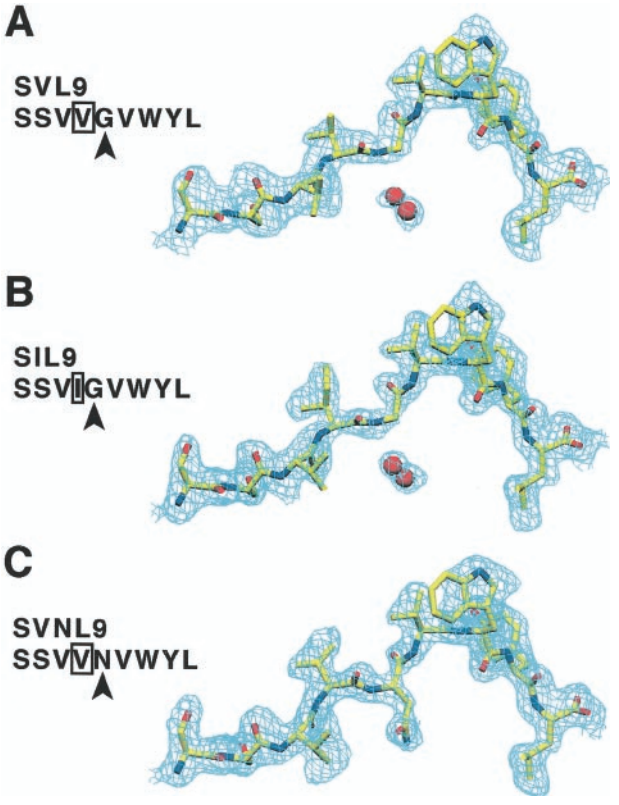

FIGURE 1. Omit electron density maps of H13 peptides. The peptides are oriented with the σ1 helix behind the plane of the page, the σ2 helix in front of the plane of the page, and the β-sheet below the peptides. *A–C*, Simulated annealing F_o-F_c maps were calculated with SVL9 (SSV VGVWYL), SIL9 (SSVIGVWYL), and SVNL9 (SSVVNVWYL) peptides and water molecules were omitted from the models. F_o-F_c maps were calculated in the CNS (14) and were contoured at 2.0 σ. Density within a radius of 1.4 Å of the peptides is displayed. C, N, and O atoms are colored yellow, blue, and red, respectively. Position 4 of the peptides are shown in boxes. Position 5 is indicated with triangles. Fig. 1 was made with SETOR (48).

Results

Water molecules fulfill the role of the anchor residue in stabilizing the C pocket of the D^b cleft

To investigate the question of how noncanonical peptides compensate for the lack of a conventional anchor residue, we solved crystal structures of D^b in complex with both allelic forms of H13: $H13^a$ (termed SVL9: SSVVGVWYL) and $H13^b$ (SIL9: SS VIGVWYL; Table I). In addition, we determined the structure of D^b complexed to a peptide analog of $H13^a$ in which we have imposed a $P5^{Asn}$ anchor residue (SVNL9: SSVVNVWYL). Omit electron density maps for the regions corresponding to the H13 peptides are shown in Fig. 1.

Two water molecules are observed in the C pocket of $H13^a$ (SVL9) and $H13^b$ (SIL9) peptide/D^b complexes (Figs. 1 and 2), which form H-bonds to C pocket side chains (Gln^{70}, Gln^{97}, and Tyr^{156}). These interactions stabilize the architecture of the groove and enable the anchorless H13 peptides to assume backbone conformations characteristic of conventionally anchored peptides.

The structural similarity between H13 peptides and canonical peptide conformation is shown in Fig. 3*A* in which the $H13^a$ peptide, SVL9, is superimposed on a D^b-bound peptide that contains the $P5^{Asn}$ anchor residue, SEV9 (FAPGNYPAL; Ref. 23). The MHC binding strategy used by the H13 peptides is distinct from that used by a previously described peptide, p1027 (FAPGVFPYM; Ref. 24), which binds D^b despite the lack of a $P5^{Asn}$ anchor by bulging in the central region of the peptide to allow the $P6^{Phe}$ side chain to serve as a new anchor (Fig. 3*B*). These results demonstrate that noncanonical peptides are capable of adopting multiple conformations to accommodate MHC binding, importantly including the conventional conformation as demonstrated by both allelic forms of H13 (Fig. 3, *A* and *C*).

Allelic discrimination of H13 epitopes depends upon the presence/absence of a single methyl group poised for TCR CDR3 recognition

The only difference between the allelic H13 peptides is the presence of either $P4^{Val}$ or $P4^{Ile}$. As shown in Fig. 4, the $P4^{Ile}$ side chain of SIL9 assumes a similar side chain rotamer conformation as $P4^{Val}$ in SVL9, with the additional methyl group (Cδ1) positioned directly between the α1 and α2 helices of D^b. $P4^{Ile}$ in the SIL9 peptide is more exposed to solvent than $P4^{Val}$ in SVL9, and is predicted to protrude directly into the central portion of the TCR-binding interface (Fig. 4*A*; Refs. 27–29). The $P4^{Val} \leftrightarrow P4^{Ile}$ substitution results in only minimal alteration in the P4 side chain at a site readily accessible to TCR contact.

Comparison of the SIL9 and SVL9 pD^b crystal structures revealed two notable differences in addition to those at the P4 side chain. First, although the H13 peptides have similar backbone conformations, the buried $P3^{Val}$ side chains exhibit alternate rotamer

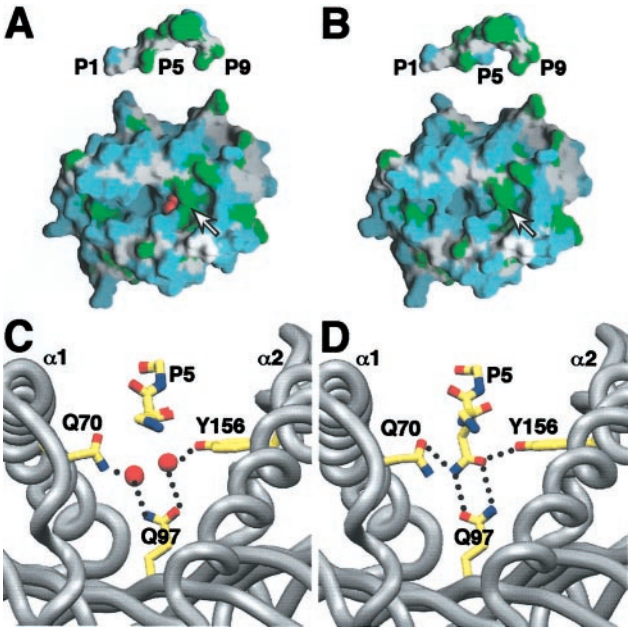

FIGURE 2. Water molecules occupy the P5 anchor site and stabilize the C pocket. The two ordered water molecules in the C pocket of the SVL9/D^b complex are shown as red spheres in *A*. The molecular surfaces depicted in *A* and *B* are colored according to side chain characteristics: blue for polar side chains and green for hydrophobic side chains. The SVL9 peptide in *A* and the SVNL9 peptide in *B* have been translated above the D^b clefts and are rotated 90° about a horizontal axis in the plane of the page. *A* and *B* were made with GRASP (49). H-bonding interactions between water molecules and side chains of C pocket residues Gln^{70}, Gln^{97}, and Tyr^{156} are depicted in *C*. *D*, The $P5^{Asn}$ anchor residue forms interactions with Gln^{70}, Gln^{97}, and Tyr^{156}. *C* and *D*, The orientation is such that C termini of the peptides are behind the plane of the page, and the N termini of the peptides are in front of the plane of the page. *C* and *D* were made with SETOR.

conformations in SIL9 compared with SVL9 (Fig. 3, *C* and *D*). Second, a H-bond between Glu^{163} and the hydroxyl group of $P1^{Ser}$ is observed in $H13^b$ (SIL9/pD^b), but not in $H13^a$ (SVL9/pD^b). This H-bond is also found in SVNL9 (Fig. 4*C*) and promotes formation of a salt bridge across the Ag binding cleft from Lys^{66} of the α1 helix to Glu^{163} of the α2 helix (Fig. 4*C*). The variability observed at Glu^{163} in pD^b crystal structures (Fig. 4*C*) suggests conformational plasticity at this site.

Mapping sites critical for T cell recognition of H13

Analysis of solvent accessibility indicates that among the H13 peptide residues, $P4^{Val/Ile}$, $P6^{Val}$, $P7^{Trp}$, and $P8^{Tyr}$ are most accessible to the TCR (17). The relative contribution of these amino acid side chains to T cell recognition and activation was analyzed. First, $LMtk^-$ cells expressing D^b cells were transfected with H13 minigenes encoding H13 peptides that have incorporated random substitutions at solvent accessible residues. T cell triggering by anti-$H13^a$ and anti-$H13^b$ T cell hybridomas was assayed to determine which mutations were tolerated by the hybridoma TCRs (Fig. 5). The anti-$H13^b$ hybridoma tolerated only Ile at P4 (Fig. 5*B*), demonstrating a stringent requirement for the Cδ1 atom of $P4^{Ile}$ in the natural SIL9 ligand. In contrast, the anti-$H13^a$ hybridoma showed a less stringent specificity, as it tolerated multiple substitutions at P4 (Fig. 5*A*). We also examined the effect of substitutions at P6–8, which bulge out of the peptide binding groove to traverse the hydrophobic ridge in the D^b cleft. Substitutions at P7 and P8, the most solvent exposed positions of the H13 peptides, were not tolerated, whereas a wide array of P6 substitutions were tolerated (data not shown). Therefore, side chains of P4, P7, and P8, but not P6 are essential components in the binding of both anti-$H13^a$ and anti-$H13^b$ TCRs.

Structural and functional effects of an imposed central anchor

The identification of antigenic T cell epitopes and the design of agonist and antagonist ligands have in large part relied on the elaboration of allele-specific binding motifs and the definition of anchor residues (30–34). Immune responses to tumor Ag peptides lacking anchor residues have been reported to be enhanced by modifications that provide a surrogate anchor (35, 36). However, the extent to which peptides with imposed anchors improve antigenicity remains uncertain. The H13 model provides a sensitive and robust system to investigate this issue. pMHC complexes rendered stable by the imposition of anchor residues would be expected to enhance antigenicity, presumably by increasing cognate pMHC density on the plasma membrane. Alternatively, peptides modified so that they have improved anchors could alter the conformation of the peptide, and in doing so, disrupt TCR binding. To test these possibilities, the effects of adding a central anchor residue to H13 peptides on MHC binding and T cell recognition were analyzed. Analysis of the crystal structures of the anchorless and anchored pD^b complexes then allowed for the correlation of functional parameters with structural alterations.

Consistent with a role for the conventional P5 anchor in pMHC stabilization, replacement of the native $P5^{Gly}$ of SVL9 with a $P5^{Asn}$ increased its affinity for D^b ~10-fold (Table I). This increased affinity is consistent with the crystal structure of SVNL9, showing that the $P5^{Asn}$ side chain participates in prototypic H-bonds with amino acid side chains of C pocket residues Gln^{70}, Gln^{97}, and Tyr^{156} (Fig. 2*D*).

To determine the consequence of $P5^{Asn}$ substitutions on CTL recognition, CTLs generated after reciprocal H13 congenic strain immunization were analyzed. As previously shown (2), allelic discrimination by normal CTLs occurs within a remarkably narrow peptide concentration range: ~1–100 pM for anti-$H13^a$ CTLs and ~1–1000 pM for anti-$H13^b$ CTLs (Fig. 5, *C* and *D*). H13 peptides substituted with $P5^{Asn}$ anchors were no more active than the naturally occurring SIL9 and SVL9 peptides in this assay (Fig. 5, *C* and *D*).

The $P5^{Asn}$-substituted peptides actually inhibited recognition by anti-$H13^a$ CTL (Fig. 4*C*), suggesting that the improved anchors induced structural changes that modified the complementarity of the anti-$H13^a$ TCR with the pMHC interface to outside the biologically optimal range. Overall, the imposed $P5^{Asn}$ anchor pulls the central portion of the SVNL9 peptide backbone more toward the α2 helix compared with SVL9 and SIL9 (0.6 Å at the Cα atoms of P4). In addition, the imposed anchor induced a change in the rotamer conformation of $P4^{Val}$ (Fig. 4*B*), the key TCR contact residue in the H13 response.

It is not clear how TCR binding affects the conformation of the anchor-imposed SVNL9 peptide. Because structures of TCR complexed to pMHC have shown that TCR binding can alter the peptide conformation (37–40), TCR binding may induce a conformational change in SVL9. One explanation that may account for the inhibited T cell response to SVNL9 is that the main chain of SVNL9 is restricted from undergoing a conformational change induced by TCR binding. Despite observed and proposed structural changes, it is important to note that allelic discrimination, i.e. the ability of the CTLs to discriminate allo-$P4^{Ile}$ from self-$P4^{Val}$ substitutions, was preserved in the context of the $P5^{Asn}$-modified H13 peptides. This is supported by the ranges of concentrations required for inducing the CTLs, which demonstrate that self and allo agonist activity was minimally affected by the $P5^{Asn}$ substitution

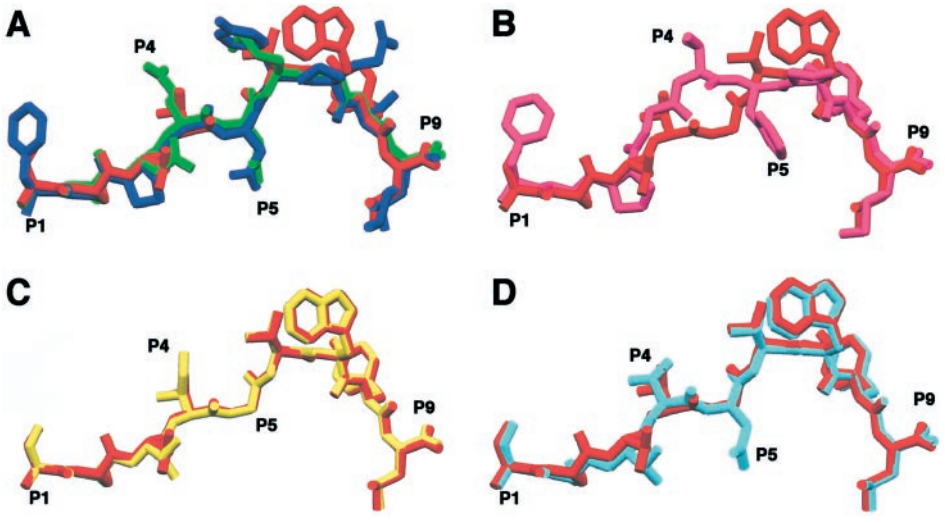

FIGURE 3. Peptide conformations of H13 peptides resemble motif-bearing peptides bound to H2-D^b. *A*, SVL9 (SSVVGVWYL), in red, is superimposed on a peptide that exhibits the conventional D^b binding motif, SEV9 (FAPGNYPAL) in blue. *B*, SVL9 is superimposed on p1027 (FAPGVFPYM), in magenta, and reveals structural variation in peptides that have incomplete MHC supermotifs. *C*, SVL9, the peptide recognized by D^b-restricted T cells specific for H13^a, is shown superimposed on SIL9 (SSVIGVWYL), the peptide recognized by D^b-restricted T cells specific for H13^b. *D*, SVL9 is superimposed on the singly substituted analog SVNL9 (SSVVNVWYL) that contains an anchoring P5^{Asn} side chain. *E*, H-bonds and solvent accessibilities are shown for motif and nonmotif pD^b structures.

E

	SVL9	SIL9	SVNL9	NP9	SEV	p1027
Buried surface area (Å^2)	1729	1719	1776	1793	1724	1744
% Buried	75.9	75.7	77.7	78.3	79.7	74.3
H-bonds between peptide and D^b	19	19	23	23	18	14
van der Waals between peptide and D^b	163	164	198	139	206	162
Waters bridging peptide and D^b	1	2	2	1	0	0
Waters bound exclusively to peptide	4	6	7	2	0	0
Resolution (Å)	2.2	2.0	1.9	2.4	2.9	2.8

(Fig. 5, *C* and *D*). In the case of anti-H13^a CTLs, the P5^{Asn} modification did not abrogate allelic discrimination, but rather acted additively to increase the concentration required to achieve equivalent levels of cytolysis. These results suggest that structural changes induced by the P5^{Asn} substitution are independent of those involved in allelic discrimination.

Discussion

The structural basis of the H13 transplantation Ag

Minor H Ags are allelically variant self peptides that pose a serious clinical concern in organ and bone marrow transplants, even under conditions of an MHC match (41). An increasing number of minor H Ags are being identified at the molecular level, but none have been examined at the structural level (42). This characterization of Snell's classical H13 Ag provides a model for understanding how the most subtle molecular changes are sensed by T cells, ultimately resulting in transplant rejection. The topologies of the H13 pMHC complexes are remarkably similar, with the most notable difference being the extension of the P4 side chain by a single methyl group in SIL9 compared with SVL9. Modeling of the 2C TCR juxtaposed onto H13 peptides suggests that while a large surface area engages the TCR CDR loops, CDR3α is positioned for direct contact with the terminal end of the P4 side chain (40). Allelic discrimination was preserved by anti-H13 CTLs, even in the context of modest reorganization of the peptide conformation imposed by the substitution of a P5^{Asn} anchor (Fig. 5, *C* and *D*), suggesting

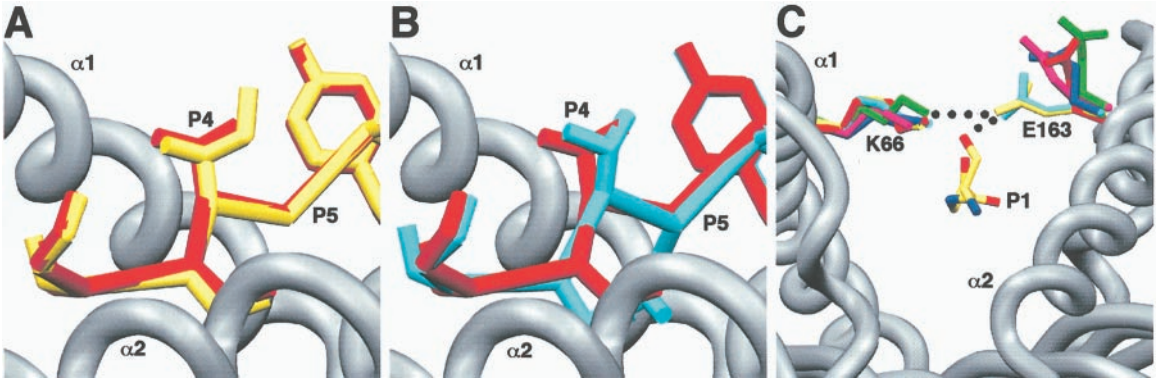

FIGURE 4. Structural differences between H13 complexes at potential TCR contacts. *A*, Superposition of SVL9 (H13^a, in red) and SIL9 (H13^b, in yellow) shows how the methyl group of P4^{Ile} in SIL9 is poised for TCR engagement. *B*, Superposition of SVL9 (H13^a, in red) and SVNL9 (H13^a with modified P5, in blue) shows how the imposed P5^{Asn} anchor results in a flip in the P3^{Val} and P4^{Val} side chain conformations, and a shift in the main chain toward the α2 helix. *C*, The salt bridge between Lys^{66} and Glu^{163} provides a mechanism to hold the peptides in the groove. The side chain conformation of Glu^{163} allows the H-bonding to hydroxyl group of P1^{Ser} and is observed in SIL9 (H13^b, in yellow) and SVNL9 (H13^a with modified P5, in sky blue) complexes with D^b, but not other structures of D^b-bound peptides: SVL9 (H13^a, in red; NP9, in green; CE6, in dark blue; and BZ9, in magenta). Fig. 5 was made with SETOR (48).

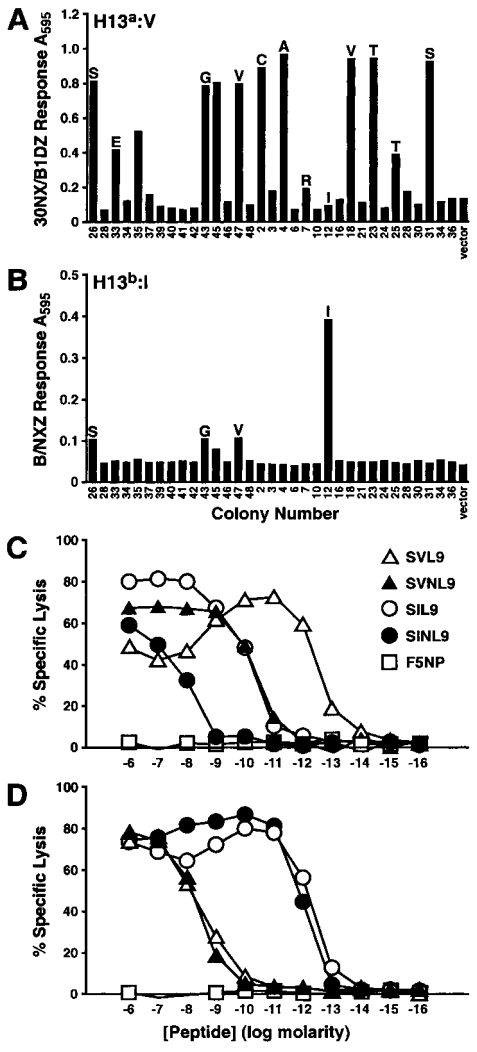

FIGURE 5. TCR sensitivity to substitutions in the polymorphic position P4 and the P5 anchor. Functional analysis of anti-H13 TCR recognition of naturally occurring and unnatural P4 and $P5^{Asn}$ anchor substitutions. *A* and *B*, Individual minigene constructs encoding random amino acid substitutions (X) at position 4 of the H13 antigenic peptide SSV(X)GVWYL were cotransfected into LMtk- cells with D^b MHC class I and B7-2 cDNA constructs as described (H47 REF). Specific recognition of the transfected LMtk cells by $H13^a$-specific T cell hybrid 30NX/B10Z *A* and the $H13^b$-specific T cell hybrid B/NXZ *B* was then measured by the *lacZ* assay. The minigene constructs were sequenced to determine the identity of the "X" residue, shown by single letter code above the bars. Duplicate transfectants were screened with the $H13^a$-specific hybrid 30NXBXZ (*A*), or the $H13^b$-specific hybrid B/NXZ (*B*). *C*, Recognition of allelic H13 peptides and $P5^{Asn}$-substituted analogs by anti-$H13^a$ CTL. *D*, Recognition of allelic H13 peptides SVL9 and SIL9 and $P5^{Asn}$-substituted analogs SVNL9 and SSV-INVWYL (SINL9) by anti-$H13^b$ CTL.

that CDR3α has sufficient flexibility to bind the $P4^{Val}$ side chain repositioned by the $P5^{Asn}$ substitution, and in doing so, trigger the TCR. X-ray crystallographic studies of agonist and superagonist pK^b ligands for the 2C11 TCR suggested that the ability to form H-bonds between CDR3 loops and a critical peptide side chain is necessary to induce optimal TCR triggering (40). The presence/absence of a single methyl group may be an even more subtle trigger in which a small number of van der Waals contacts between the TCR CDR3α and the P4 side chain forms the basis of H13 allelic discrimination.

However, it is also possible that TCRs specific for $H13^a$ recognize SVL9 in a way that alters the peptide conformation, which can occur with valine and other side chains (Fig. 4*A*), but not isoleucine. Structures of TCR complexed to pMHC have shown that TCR binding can distort the peptide conformation (37–40). The crystal structures of H13 specific TCRs bound to respective ligands may assist in distinguishing these possibilities.

Anchor imposition decreases antigenicity by causing conformational changes in a key TCR contact residue

Allele-specific MHC motifs have been a lynchpin of antigenic epitope definition and peptide-based vaccine design. Previous studies have all been consistent with obligate contacts between central anchor residues and MHC, either by direct interaction or by water-mediated H-bonds. Water molecules are frequently observed to fill cavities at molecular interfaces such as the TCR/pMHC interface (43) and the peptide/MHC interface (25). Because the loss of a single H-bond can decrease affinity by several orders of magnitude (44), direct or water-mediated H-bonds between anchor residues and MHC have been previously thought to be necessary for display of the characteristic peptide backbone configurations for each specific MHC allele (6, 7). However, some naturally occurring peptides, including the non-MHC encoded H Ags H13 (2) and H47 (45), are immunogenic despite the lack of a canonical central anchor residue. A clearer understanding of how such nonmotif peptides accomplish this task is a matter of considerable importance. In this report, we show two unprecedented features of the naturally occurring nonmotif H13 peptides (containing $P5^{Gly}$ instead of $P5^{Asn}$): neither direct nor water-mediated H-bond interactions bridge anchor residues and MHC; and they assume the prototypic backbone structure for D^b motif-bearing peptides. Thus, our studies provide evidence that interactions between central anchor residues and MHC side chains are not necessary for Ag presentation to T cells. In addition, the ability of water to stabilize the C pocket without the assistance of a peptide side chain has implications on the initial formation of pMHC complexes in the endoplasmic reticulum as well as intra- and extracellular peptide exchange.

Innovative insights into unresolved problems associated with modification of T cell epitopes are provided by the structure and function of an anchor-modified minor H Ag (Figs. 1*D*, 2*B*, 3, *B* and *D*, 4, and 5*B*). The extent to which peptides can be improved as immunogens by modification of anchor residues is a significant unresolved issue. Although vaccination of melanoma patients with an anchor-imposed peptide derived from the gp100 melanoma-associated Ag, $gp100_{209-2\,M}$, was reported to be significantly more efficient in generating clinical responses to melanoma in clinical trials (46), a study assessing the effect of modified anchors on melanoma-reactive CTL reported that only 2 of 47 modified peptides actually increased binding, immunogenicity, and recognition by established CTL lines (47). X-ray crystallographic analysis of the H13 SVNL9 pD^b complex indicates that the $P5^{Asn}$ side chain is engaged in prototypic H-bond contacts with the D^b C pocket, which can account for the increased stability of the SNVL9 pD^b complex compared with that of the SVL9 pD^b (Table I). However, despite substantially increased binding, structural changes induced by the $P5^{Asn}$ anchor not only failed to increase agonist activity, but for SVL9 pD^b, the $P5^{Asn}$ substitution went so far as to reduce agonist activity of the SVL9 pD^b complex (Fig. 4*C*). Our results provide the first direct structural evidence that anchor imposition decreases antigenicity by causing subtle conformational changes in critical TCR contact residues of the peptide. Careful consideration of the consequences of anchor residues and water in peptide-MHC interactions should assist in epitope identification and vaccine design.

Acknowledgments

We thank Zbgniew Dauter for use of x-ray facilities, Shari Roopenian for excellent technical assistance, and David Serreze for critical review of the manuscript.

References

1. Snell, G. D., G. Cudkowicz, and H. P. Bunker. 1967. Histocompatibility genes of mice. VII. H-13, a new histocompatibility locus in the fifth linkage group. *Transplantation 5:492.*
2. Mendoza, L. M., P. Paz, A. Zuberi, G. Christianson, D. Roopenian, and N. Shastri. 1997. Minors held by majors: the H13 minor histocompatibility locus defined as a peptide/MHC class I complex. *Immunity 7:461.*
3. Falk, K., O. Rotzschke, and H. G. Rammensee. 1990. Cellular peptide composition governed by major histocompatibility complex class I molecules. *Nature 348:248.*
4. Falk, K., O. Rotzschke, S. Stevanovic, G. Jung, and H. G. Rammensee. 1991. Allele-specific motifs revealed by sequencing of self-peptides eluted from MHC molecules. *Nature 351:290.*
5. Rotzschke, O., K. Falk, K. Deres, H. Schild, M. Norda, J. Metzger, G. Jung, and H. G. Rammensee. 1990. Isolation and analysis of naturally processed viral peptides as recognized by cytotoxic T cells. *Nature 348:252.*
6. Wilson, I. A., and D. H. Fremont. 1993. Structural analysis of MHC class I molecules with bound peptide antigens. *Semin. Immunol. 5:75.*
7. Madden, D. R. 1995. The three-dimensional structure of peptide-MHC complexes. *Annu. Rev. Immunol. 13:587.*
8. Fremont, D. H., M. Matsumura, E. A. Stura, P. A. Peterson, and I. A. Wilson. 1992. Crystal structures of two viral peptides in complex with murine MHC class I H-2K^b. *Science 257:919.*
9. Matsumura, M., D. H. Fremont, P. A. Peterson, and I. A. Wilson. 1992. Emerging principles for the recognition of peptide antigens by MHC class I molecules. *Science 257:927.*
10. Young, A. C., W. Zhang, J. C. Sacchettini, and S. G. Nathenson. 1994. The three-dimensional structure of H-2D^b at 2.4 Å resolution: implications for antigen-determinant selection. *Cell 76:39.*
11. Jancarik, J., W. G. Scott, D. L. Milligan, D. E. J. Koshland, and S. H. Kim. 1991. Crystallization and preliminary x-ray diffraction study of the ligand-binding domain of the bacterial chemotaxis-mediating aspartate receptor of *Salmonella typhimurium*. *J. Mol. Biol. 221:31.*
12. Minor, W., D. Tomchick, and Z. Otwinowski. 2000. Strategies for macromolecular synchrotron crystallography. *Struct. Fold Des. 8:R105.*
13. Navaza, J., E. H. Panepucci, and C. Martin. 1998. On the use of strong Patterson function signals in many-body molecular replacement. *Acta Crystallogr. D Biol. Crystallogr. 54(Pt. 5):817.*
14. Brunger, A. T., P. D. Adams, G. M. Clore, W. L. DeLano, P. Gros, R. W. Grosse-Kunstleve, J. S. Jiang, J. Kuszewski, M. Nilges, N. S. Pannu et al. 1998. Crystallography & NMR system: a new software suite for macromolecular structure determination. *Acta Crystallogr. D Biol. Crystallogr. 54(Pt. 5):905.*
15. Jones, T. A., J. Y. Zou, S. W. Cowan, and M. Kjeldgaard. 1991. Improved methods for binding protein models in electron density maps and the location of errors in these models. *Acta Crystallogr. 47(Pt. 2):110.*
16. Laskowski, R. A., D. S. Moss, and J. M. Thornton. 1993. Main-chain bond lengths and bond angles in protein structures. *J. Mol. Biol. 231:1049.*
17. Kabsch, W., and C. Sander. 1983. Dictionary of protein secondary structure: pattern recognition of hydrogen-bonded and geometrical features. *Biopolymers 22:2577.*
18. Jones, S., and J. M. Thornton. 1996. Principles of protein-protein interactions. *Proc. Natl. Acad. Sci. USA 93:13.*
19. McDonald, I. K., and J. M. Thornton. 1994. Satisfying hydrogen bonding potential in proteins. *J. Mol. Biol. 238:777.*
20. Sheriff, S., W. A. Hendrickson, and J. L. Smith. 1987. Structure of myohemerythrin in the azidomet state at 1.7/1.3 Å resolution. *J. Mol. Biol. 197:273.*
21. Franco, A., T. Yokoyama, D. Huynh, C. Thomson, S. G. Nathenson, and H. M. Grey. 1999. Fine specificity and MHC restriction of trinitrophenyl-specific CTL. *J. Immunol. 162:3388.*
22. Mendoza, L. M., Villaflor, G., Eden, P., Roopenian, D., and N. Shastri. 2001. Distinguishing self from nonself: immunogenicity of the murine H47 locus is determined by a single amino acid substitution in an unusual peptide. *J. Immunol. 166:4438.*
23. Sanderson, S., and N. Shastri. 1994. *LacZ* inducible, antigen/MHC-specific T cell hybrids. *Int. Immunol. 6:369.*
24. Roopenian, D. C., A. P. Davis, G. J. Christianson, and L. E. Mobraaten. 1993. The functional basis of minor histocompatibility loci. *J. Immunol. 151:4595.*
25. Glithero, A., J. Tormo, J. S. Haurum, G. Arsequell, G. Valencia, J. Edwards, S. Springer, A. Townsend, Y. L. Pao, M. Wormald et al. 1999. Crystal structures of two H-2D^b/glycopeptide complexes suggest a molecular basis for CTL cross-reactivity. *Immunity 10:63.*
26. Zhao, R., D. J. Loftus, E. Appella, and E. J. Collins. 1999. Structural evidence of T cell xeno-reactivity in the absence of molecular mimicry. *J. Exp. Med. 189:359.*
27. Garcia, K. C., M. Degano, R. L. Stanfield, A. Brunmark, M. R. Jackson, P. A. Peterson, L. Teyton, and I. A. Wilson. 1996. An $\alpha\beta$ T cell receptor structure at 2.5 A and its orientation in the TCR-MHC complex. *Science 274:209.*
28. Garcia, K. C., M. Degano, L. R. Pease, M. Huang, P. A. Peterson, L. Teyton, and I. A. Wilson. 1998. Structural basis of plasticity in T cell receptor recognition of a self peptide-MHC antigen. *Science 279:1166.*
29. Garboczi, D. N., and W. E. Biddison. 1999. Shapes of MHC restriction. *Immunity 10:1.*
30. Calin-Laurens, V., M. C. Trescol-Biemont, D. Gerlier, and C. Rabourdin-Combe. 1993. Can one predict antigenic peptides for MHC class I-restricted cytotoxic T lymphocytes useful for vaccination? *Vaccine 11:974.*
31. Celis, E., A. Sette, and H. M. Grey. 1995. Epitope selection and development of peptide based vaccines to treat cancer. *Sem. Cancer Biol. 6:329.*
32. Chesnut, R. W., A. Sette, E. Celis, P. Wentworth, R. T. Kubo, J. Alexander, G. Ishioka, A. Vitiello, and H. M. Grey. 1995. Design and testing of peptide-based cytotoxic T-cell-mediated immunotherapeutics to treat infectious diseases and cancer. *Pharm. Biotechnol. 6:847.*
33. Sidney, J., H. M. Grey, R. T. Kubo, and A. Sette. 1996. Practical, biochemical and evolutionary implications of the discovery of HLA class I supermotifs. *Immunol. Today 17:261.*
34. Zugel, U., R. Wang, G. Shih, A. Sette, J. Alexander, and H. M. Grey. 1998. Termination of peripheral tolerance to a T cell epitope by heteroclitic antigen analogues. *J. Immunol. 161:1705.*
35. Clay, T. M., M. C. Custer, M. D. McKee, M. Parkhurst, P. F. Robbins, K. Kerstann, J. Wunderlich, S. A. Rosenberg, and M. I. Nishimura. 1999. Changes in the fine specificity of gp100 (209–217)-reactive T cells in patients following vaccination with a peptide modified at an HLA-A2.1 anchor residue. *J. Immunol. 162:1749.*
36. Bristol, J. A., J. Schlom, and S. I. Abrams. 1998. Development of a murine mutant Ras CD8$^+$ CTL peptide epitope variant that possesses enhanced MHC class I binding and immunogenic properties. *J. Immunol. 160:2433.*
37. Garboczi, D. N., P. Ghosh, U. Utz, Q. R. Fan, W. E. Biddison, and D. C. Wiley. 1996. Structure of the complex between human T-cell receptor, viral peptide and HLA-A2. *Nature 384:134.*
38. Ding, Y. H., K. J. Smith, D. N. Garboczi, U. Utz, W. E. Biddison, and D. C. Wiley. 1998. Two human T cell receptors bind in a similar diagonal mode to the HLA-A2/Tax peptide complex using different TCR amino acids. *Immunity 8:403.*
39. Ding, Y. H., B. M. Baker, D. N. Garboczi, W. E. Biddison, and D. C. Wiley. 1999. Four A6-TCR/peptide/HLA-A2 structures that generate very different T cell signals are nearly identical. *Immunity 11:45.*
40. Degano, M., K. C. Garcia, V. Apostolopoulos, M. G. Rudolph, L. Teyton, and I. A. Wilson. 2000. A functional hot spot for antigen recognition in a superagonist TCR/MHC complex. *Immunity 12:251.*
41. Petersdorf, E. W., E. M. Mickelson, C. Anasetti, P. J. Martin, A. E. Woolfrey, and J. A. Hansen. 1999. Effect of HLA mismatches on the outcome of hematopoietic transplants. *Curr. Opin. Immunol. 11:521.*
42. Roopenian, D. C., and E. Simpson. 2000. *Minor Histocompatibility Antigens: From the Laboratory to the Clinic*. Landes Bioscience, Georgetown, TX.
43. Reiser, J. B., C. Darnault, A. Guimezanes, C. Gregoire, T. Mosser, A. M. Schmitt-Verhulst, J. C. Fontecilla-Camps, B. Malissen, D. Housset, and G. Mazza. 2000. Crystal structure of a T cell receptor bound to an allogeneic MHC molecule. *Nat. Immunol. 1:291.*
44. Chacko, S., E. Silverton, L. Kam-Morgan, S. Smith-Gill, G. Cohen, and D. Davies. 1995. Structure of an antibody-lysozyme complex unexpected effect of conservative mutation. *J. Mol. Biol. 245:261.*
45. Choi, E. Y., Y. Yoshimura, G. J. Christianson, T. J. Sproule, S. Malarkannan, N. Shastri, S. Joyce, and D. C. Roopenian. 2001. Quantitative analysis of the immune response to mouse non-MHC transplantation antigens in vivo: the H60 histocompatibility antigen dominates over all others. *J. Immunol. 166:4370.*
46. Rosenberg, S. A., J. C. Yang, D. J. Schwartzentruber, P. Hwu, F. M. Marincola, S. L. Topalian, N. P. Restifo, M. E. Dudley, S. L. Schwarz, P. J. Spiess et al. 1998. Immunologic and therapeutic evaluation of a synthetic peptide vaccine for the treatment of patients with metastatic melanoma. *Nat. Med. 4:321.*
47. Parkhurst, M. R., M. L. Salgaller, S. Southwood, P. F. Robbins, A. Sette, S. A. Rosenberg, and Y. Kawakami. 1996. Improved induction of melanoma-reactive CTL with peptides from the melanoma antigen gp100 modified at HLA-A*0201-binding residues. *J. Immunol. 157:2539.*
48. Evans, S. V. 1993. SETOR: hardware-lighted three-dimensional solid model representations of macromolecules. *J. Mol. Graphics 11:134.*
49. Nicholls, A., K. A. Sharp, and B. Honig. 1991. Protein folding and association: insights from the interfacial and thermodynamic properties of hydrocarbons. *Proteins 11:281.*